INSTITUTE OF PHYSICS PUBLISHING JOURNAL OF MICROMECHANICS AND MICROENGINEERING

J. Micromech. Microeng. **16** (2006) S211–S219 doi:10.1088/0960-1317/16/9/S07

Development of a large-entrainment-ratio axisymmetric supersonic ejector for micro butane combustor

Yong Fan, Yuji Suzuki and Nobuhide Kasagi

Department of Mechanical Engineering, The University of Tokyo, 7-3-1 Hongo, Bunkyo-ku, Tokyo 113-8656, Japan

E-mail: fan@thtlab.t.u-tokyo.ac.jp

Received 17 January 2006, in final form 11 June 2006
Published 9 August 2006
Online at stacks.iop.org/JMM/16/S211

Abstract

A large-entrainment-ratio micro ejector has been developed to supply fuel–air mixture for a micro butane combustor. As a key component of the ejector, an axisymmetric convergent–divergent supersonic nozzle having a throat diameter of 42 μm is fabricated with high-precision electro-discharge machining. Operating conditions and geometric parameters of the ejector are systematically changed, and their effects on volume–flow-rate ratio are investigated in a series of experiments. Experimental data are compared with analytic solutions and CFD results. It is found that the present micro ejector achieves a maximum air-to-butane volume–flow-rate ratio of 43 when the back pressure is 11.6 Pa. It is also found that the present ejector can produce larger volume–flow-rate ratio than the previous MEMS 2D ejector at small back pressure.

1. Introduction

Due to the recent popularization of mobile electronic devices, demand for portable power sources is growing drastically. Since these electronic devices are rapidly evolving to have more functions, higher performance and prolonged duration, state-of-the-art battery technology faces a severe challenge due to insufficient energy density. Compared with batteries, hydrocarbon fuels such as butane and propane have 100 times larger energy density. Power MEMS devices, taking advantage of converting the chemical energy of hydrocarbon fuels to electricity, have shown strong commercial potential as an alternative portable power source in the future. Various power generation concepts such as MEMS gas turbine [1], micro rotary IC engine [2], micro fuel cell [3, 4] and micro thermoelectric generator [5] have been proposed. Since most of these systems except μDMFC take the approach of converting the thermal energy, which is harvested from fuel combustion, to electric energy, micro devices for feeding fuel and air to the combustor with minimal external power are one of the key components.

Figure 1 shows the concept of the present micro heat generation system. A micro nozzle is plugged into the inlet tube of a micro combustor to form an ejector. The ejector pumps ambient air to the combustion chamber by utilizing the vapor pressure of liquefied fuel. Combustion of the fuel then takes place, and heat generated is used in micro power devices such as the micro engine, fuel processor and thermoelectric generator attached to the combustor. In our separate studies [6, 7], we developed a micro catalytic combustor with nano-porous alumina catalyst support using high-precision ceramic tape casting technology. We employ butane as the fuel, because it has both high energy density (48 960 kJ kg^{-1}) and favorable storage properties due to its moderate vapor pressure at room temperature of 0.24 MPa.

The ejector, also known as a jet pump, is a pumping device that exchanges momentum between high-velocity primary flow and low-velocity secondary flow to produce a mixed flow with intermediate velocity. As shown in figure 2, acceleration of the secondary flow results in the emergence of a low-pressure area downstream of the inlet of the secondary flow, and the ambient fluid is continuously introduced into the ejector by the positive pressure gradient.

The ejector is widely employed for various industrial applications, such as deep well oil extraction, noise reduction and thrust augmentation for aircraft engines [8], and high-performance compression refrigeration systems without an expansion valve [9]. The advantage of using an ejector in the micro heat generation system is that air supply is achieved

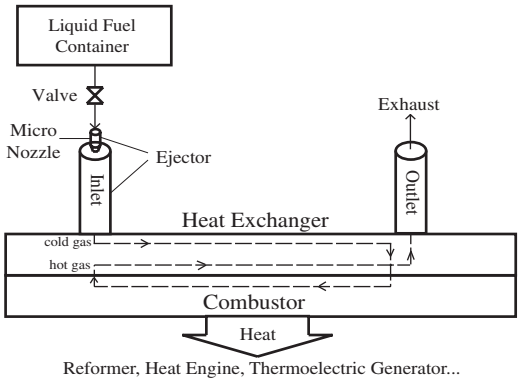

Figure 1. Micro heat generation system with ejector.

without an additional compressed air container or micro pump, and thus the system should be simple, safe and reliable.

However, the requirements on the ejector as a fuel–air feeding device for a micro combustor are completely different from conventional ejectors. First of all, the air-to-fuel volume–flow-rate ratio must be much larger than unity for the stoichiometry condition. For butane combustion, the volume–flow-rate ratio should be larger than 31. Moreover, the outlet pressure must be higher than the air inlet pressure, so that the ejector has to deliver the mixture of air and fuel against the back pressure.

Satoh *et al* [10, 11] investigated the use of a MEMS ejector as a fuel–air feeding device for a micro combustor. The ejector is fabricated by deep reactive ion etching of silicon wafers, to make 2D micro nozzles and channels. They report that the volume–flow-rate ratio, which is defined as the ratio of volume flow rates between the secondary and the primary flows, is much increased when the primary flow becomes supersonic with a micro convergent–divergent nozzle. However, 2D ejectors should suffer from large friction loss on the top and bottom channel walls. An ejector having axisymmetric structure could possibly reduce the wall friction loss, but it is not a straightforward process to accomplish axisymmetric structure with planar MEMS technologies.

The objectives of the present study are to develop a micro ejector with an axisymmetric micro nozzle by high-precision electro-discharge machining, and to evaluate its performance in a series of experiments.

2. Design of micro ejector

2.1. Quasi-1D calculation

2.1.1. 1D modeling of ejector. In order to estimate the ejector characteristic for various operating parameters as well as to give a range of these parameters for actual design, we adopted a quasi-1D calculation for constant cross-sectional area [10–12]. To provide continuity, a set of basic equations and main results are reproduced below. As shown in figure 3, we assume piecewise uniform flows at the inlet and uniform flow at the outlet. By neglecting the wall shear stresses and any energy loss, equations of continuity, momentum conservation and energy conservation can be applied to the control volume shown in figure 3.

The continuity equation is given by

$$\rho_p A_p V_p + \rho_s A_s V_s = \rho_m A_m V_m, \tag{1}$$

where ρ, A and V are respectively fluid density, cross sectional area and flow velocity. Subscripts p, s and m respectively correspond to quantities of the primary, secondary and mixed flows. The momentum equation is given by

$$P_p A_p + W_p V_p + P_s A_s + W_s V_s = P_m A_m + W_m V_m, \tag{2}$$

where P is the gauge static pressure. Mass flow rate W is defined as $W = \rho AV$. The static pressure for the mixed flow P_m corresponds to the back pressure of the ejector. The energy equation is given by

$$W_p h_p + W_s h_s = W_m h_m. \tag{3}$$

In equation (3), h is the enthalpy given by

$$h = [\gamma/(\gamma - 1)](P + P_a)/\rho + V^2/2, \tag{4}$$

where γ is the specific heat ratio, and P_a is the atmospheric pressure. When introducing two dimensionless parameters, i.e., area ratio $\alpha = A_s/A_p$ and volume–flow-rate ratio $\mu = A_s V_s/(A_p V_p)$, the specific heat ratio of mixed flow can be expressed according to Dalton's law of partial pressure as

$$\gamma_m = \left(1 - \frac{\gamma_p - 1}{\gamma_p} \frac{1 + \mu \frac{\rho_s}{\rho_p} \frac{M_{Wp}}{M_{Ws}}}{1 + \mu \frac{\rho_s}{\rho_p} \frac{\gamma_s}{\gamma_p} \frac{\gamma_p - 1}{\gamma_s - 1} \frac{M_{Wp}}{M_{Ws}}}\right)^{-1}, \tag{5}$$

where M_W is the molecular weight of gas. By assuming that the static pressure of the primary and secondary flows is the same at the inlet, the primary and secondary static pressures can be expressed as

$$P_p = P_s = -\rho_s V_s^2/2, \tag{6}$$

according to Bernoulli's law.

Equation (3) can be rewritten as

$$\left(\frac{\gamma_p}{\gamma_p - 1} \frac{P_p + P_a}{\rho_p} + \frac{1}{2} V_p^2\right) + \mu \frac{\rho_s}{\rho_p} \left(\frac{\gamma_s}{\gamma_s - 1} \frac{P_s + P_a}{\rho_s} + \frac{1}{2} V_p^2 \left(\frac{\mu}{\alpha}\right)^2\right) = \left(1 + \mu \frac{\rho_s}{\rho_p}\right) \left(\frac{\gamma_m}{\gamma_m - 1} (P_m + P_a) \frac{1}{\rho_m} + \frac{1}{2} V_m^2\right), \tag{7}$$

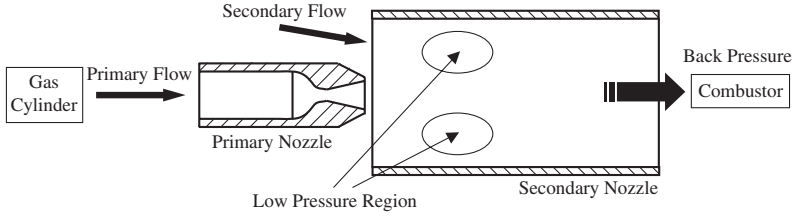

Figure 2. Schematic of ejector for micro combustor.

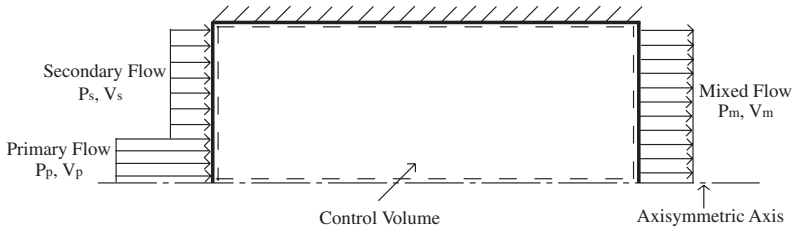

Figure 3. Control volume in quasi-1D calculation.

where ρ_m and V_m^2 can be derived from equations (1) and (2) as

$$\frac{1}{\rho_m} = A_m \frac{\left(P_p + \rho_p V_p^2\right)A_p + \left(P_s + \rho_s V_s^2\right)A_s - P_m A_m}{(\rho_p V_p A_p + \rho_s V_s A_s)^2}, \quad (8)$$

$$V_m^2 = \frac{\left[\left(P_p + \rho_p V_p^2\right)A_p + \left(P_s + \rho_s V_s^2\right)A_s - P_m A_m\right]^2}{(\rho_p V_p A_p + \rho_s V_s A_s)^2}. \quad (9)$$

In equations (8) and (9), area and velocity can be expressed by dimensionless parameters α and μ.

The relationship between the volume–flow-rate ratio μ and the area ratio α for a given back pressure P_m can be obtained by manipulating equations (5)–(9). As already reported in previous studies [10, 11], for a given back pressure, the volume–flow-rate ratio firstly increases with the area ratio, and then decreases after it reaches its maximal value. The back pressure has a strong effect on the volume–flow-rate ratio; volume–flow-rate ratio rapidly decreases with increasing back pressure. The area ratio at the optimal point, where the volume–flow-rate ratio reaches its maximum, becomes smaller for large back pressure. When the area ratio is large, tolerance to the back pressure is deteriorated. For butane, the proper range of the area ratio is about 350–2000 when the volume–flow-rate ratio is targeted at 31 for back pressures up to 100 Pa. It is found that for given primary and back pressures, the volume–flow-rate ratio for air as the primary flow source is smaller than that for butane due to its smaller molecular weight.

2.1.2. 1D modeling of primary nozzle. The flow in the primary nozzle having convergent–divergent contour is modeled with a quasi-1D isentropic assumption. When the primary nozzle works under the supersonic condition, the primary mass flow rate W_p can be expressed by a function of nozzle throat diameter D_{throat} and primary total pressure P_{Tp} as

$$W_p = \frac{\pi}{4} D_{throat}^2 [P_{Tp} + P_a] \sqrt{\frac{\gamma_p}{RT_0}\left(\frac{2}{\gamma_p + 1}\right)^{\frac{\gamma_p+1}{\gamma_p-1}}}, \quad (10)$$

where R and T_0 are respectively the gas constant and the total temperature. With this formula, we set the throat diameter of the primary nozzle to 42 μm, which produces a butane mass flow rate of about 0.84×10^{-6} kg s^{-1} for P_{Tp} equals 0.1 MPa, corresponding to a gross heat of combustion of about 38 W.

For a convergent–divergent nozzle, the exit flow condition depends not only on the ratio of nozzle exit area and throat area, but also on the pressure ratio of upstream and downstream flows. However, the nozzle should be designed in such a way that the exit pressure equals the surrounding pressure, and the flow inside the nozzle is isentropic without any shock waves, and becomes supersonic. Under such condition, the ratio of nozzle exit area and throat area can be given by exit Mach number Ma and gas specific heat ratio γ as

$$\frac{A_{exit}}{A_{throat}} = \frac{1}{Ma}\left[\frac{2}{\gamma_p + 1}\left(1 + \frac{\gamma_p - 1}{2} Ma^2\right)\right]^{\frac{\gamma_p+1}{2(\gamma_p-1)}}. \quad (11)$$

In equation (11), we assume an exit Mach number of 2, and this gives a nozzle exit diameter of 60 μm. It is noted that the exit Mach number also depends on the total pressure.

2.2. CFD simulation

Micro nozzles are of increasing interest in space propulsion to provide orbital maneuvering for small-scale satellites [13, 14]. Characteristics of micro-scale jet flows are large viscous loss due to low Reynolds numbers and the rarefied gas effect due to large Knudsen number. Bayt and Breuer [15] examined the viscous effect in jet flows issued from micro nozzles having a throat width of 19 μm. Flow visualization in a supersonic micro nozzle having throat diameter down to 1 mm has also been conducted with the aid of molecular tagging velocimetry [16]. Wang and Li [17] employed a DSMC method to predict the performance of micro nozzles. Their simulation results have shown that, unlike in the macroscale nozzles, the flow becomes supersonic downstream of the throat, but dissipates to subsonic rapidly. Hao and Ding [18] adopted a dimensional analysis and pointed out that the higher viscous dissipation in micro nozzles having larger surface-to-volume ratio contributes to the diminution of the supersonic region downstream.

However, unlike the present micro nozzle working under atmospheric pressure, previous experimental data and related numerical simulation results are limited to the case that the working gas expands into a vacuum environment. In the present study, we employ CFD software (Fluent 6) to make a preliminary analysis of the flow field inside the ejector.

CFD analysis of compressible flow is conducted to solve momentum and species transport equations in a 2D axisymmetric computational domain. Detailed dimensions of the domain are taken from the actual ejector. As described above, the throat and exit diameters of the present nozzle are respectively 42 μm and 60 μm, and the expansion angle is chosen as 10°. The total pressure of butane at the inlet of the primary nozzle and the static pressure of air at the outlet are given as boundary conditions. Atmospheric pressure is assumed at the inlet of the secondary nozzle. The wall temperature is kept constant at 300 K. Note that the effect of heat exchange between the working fluid and the wall is confirmed to be minor in the present study.

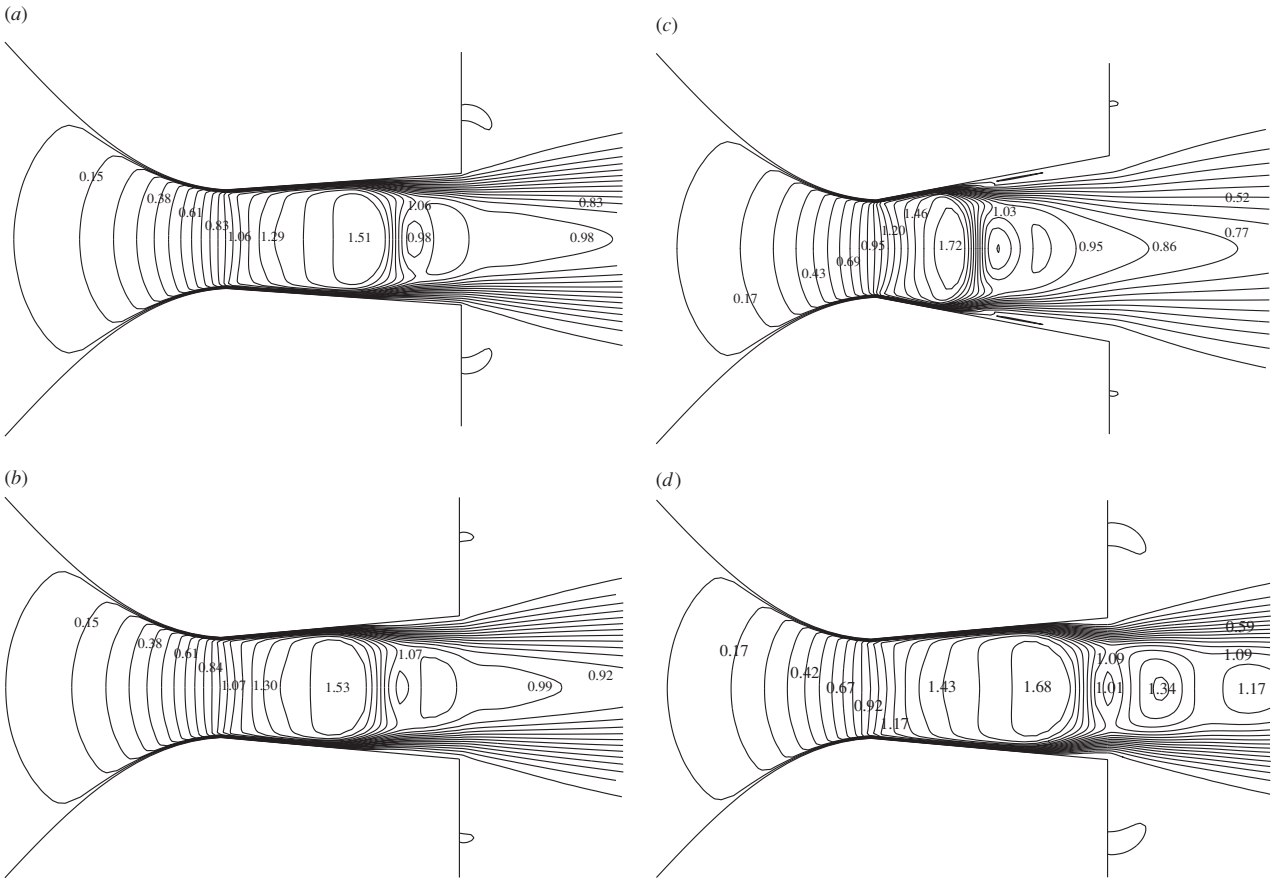

Figure 4. Contours of the Mach number in the primary nozzles with different configurations. (*a*) Nozzle design with an expansion angle of 8°, $P_{TP} = 0.1$ MPa; (*b*) present design (expansion angle = 10°), $P_{TP} = 0.1$ MPa; (*c*) nozzle design with a expansion angle of 21.5°, $P_{TP} = 0.1$ MPa; (*d*) present design (expansion angle = 10°), $P_{TP} = 0.16$ MPa.

The Knudsen number at the throat is around 0.002, so that the rarefied gas effect should be minor. The throat Reynolds number for supersonic flow is around 3600, and thus a turbulence model should be used near the nozzle exit, where the jet flow becomes unsteady and probably turbulent. In the present study, the standard k–ε turbulence model [19] is employed as the first-order estimation. For the primary butane jet, the Reynolds number at the nozzle exit is about 5000, so that the jet should be turbulent. On the other hand, the Reynolds number near the exit is about 1000, and relaminalization should occur in the secondary nozzle. Since the standard k–ε model cannot predict the relaminalization, the present simulation should overestimate the Reynolds shear stress and thus the mixing between primary and secondary flows. It is noted that for this type of flow, the so-called low-Reynolds-number k–ε models [20], which are unfortunately unavailable in the present CFD code, should give a better prediction.

Grid dependence is examined systematically using preliminary simulations with 130 × 60, 230 × 120 and 360 × 180 grid systems. For an area ratio of 3116, gauge primary total pressure of 0.1 MPa and back pressure of 10 Pa, the 130 × 60 grid system gives 6% difference in the volume–flow-rate ratio compared with that of the 360 × 180 grid system, while the 230 × 120 grid system gives only 1% difference. Accordingly, the grid system of 230 × 120 is finally adopted in all the present CFD simulations. It is noted, however, that the present grid system is still too coarse to capture shock waves, which might emerge even inside the primary nozzle.

Inlet boundary conditions of the turbulent kinetic energy k and dissipation rate ε are given with dimensional analysis as follows:

$$k \sim u'^2, \tag{12}$$

$$\varepsilon \sim u'^3/l, \tag{13}$$

where u' is the root-mean-square value of the velocity fluctuations, and l is the length scale of energy-containing eddies [21]. In the present study, we assume that $u' = 0.01U$ and $l = d$, where U and d are the bulk mean velocity and the nozzle diameter, respectively. The computational dependence on ε is examined by varying it to one order larger and smaller, and the volume–flow-rate ratios in these three cases are found to agree within 0.1%.

Figure 4 shows Mach number contours in the primary nozzles having expansion angles of 8°, 10° and 21.5° when the primary total pressure is 0.1 MPa or 0.16 MPa. The Mach number at the throat is somewhat smaller than unity. Unlike the macroscale convergent–divergent nozzles, which produce a supersonic flow accelerated downstream, the supersonic flow in microscale convergent–divergent nozzles is restricted to

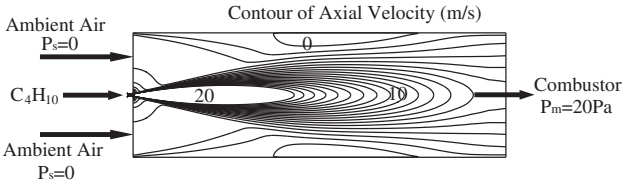

Figure 5. Contours of the axial velocity.

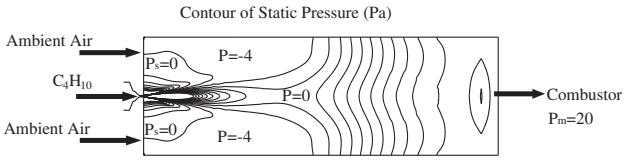

Figure 6. Contours of the static pressure.

the area between the throat and the exit, and decelerates to subsonic gradually downstream. These phenomena are also reported by Wang and Li [17] and Hao *et al* [18]. Hao *et al* claimed that the ratio of viscous dissipation to total energy is inversely proportional to the length scale, so that the viscous dissipation becomes stronger in microscale nozzles. And they attributed higher viscous dissipation to microscale nozzles as compared to that in macroscale nozzles. Therefore, nozzle design with a shorter divergent section, which causes less friction loss, may be superior for supersonic micro nozzles. In the present design having an expansion angle of 10° shown in figure 4(*b*), a maximum Mach number of $Ma = 1.53$ is achieved inside the nozzle, and the nozzle exit Mach number in the center is close to unity. It is shown in figure 4(*a*) that a nozzle having a small expansion angle of 8° produces a slightly smaller Mach number. On the other hand, serious flow separation occurs in the nozzle having a larger expansion angle of 21.5° as shown in figure 4(*c*), and the Mach number is below unity in a large portion of the exit. It is also shown in figures 4(*a*)–(*c*) that the supersonic region is mainly confined to the divergent section when the inlet total pressure is 0.1 MPa. By increasing the total pressure to 0.16 MPa (figure 4(*d*)), the supersonic region moves downstream. It is found that the 'core' region, which contains the region with the maximum Mach number, could finally extend beyond the nozzle exit when the total pressure is around 0.2 MPa (not shown). It is conjectured that the effect of viscous dissipation becomes weaker with increasing total pressure.

It is shown in the contours of the axial velocity (figure 5) that the mean velocity at the secondary nozzle exit is about 5 m s^{-1}, which corresponds to a Reynolds number of about 1000. As mentioned above, considerable variation of the Reynolds number in different regions of the ejector indicates that the standard k–ε turbulence model is not optimum for the simulation. Figure 6 shows the contours of the static pressure. Low-pressure regions emerge downstream of the secondary inlet, which forms a positive pressure gradient driving the secondary flow into the ejector.

Figure 7 shows the radial distribution of butane for the primary total pressure of 0.1 MPa and 0.16 MPa. It is found 8 mm downstream of the inlet of the secondary nozzle that the butane concentration is almost uniformly distributed in the

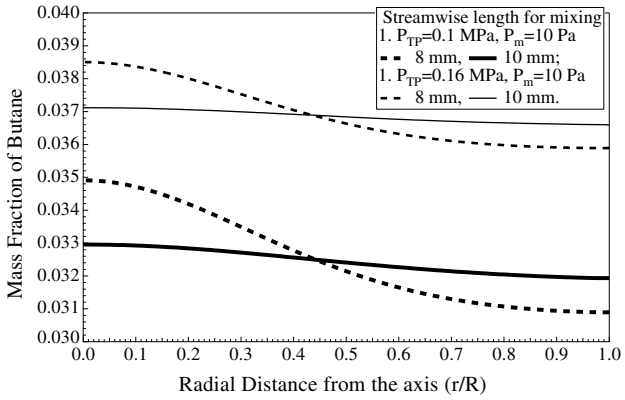

Figure 7. Radial distribution of mass fraction of butane.

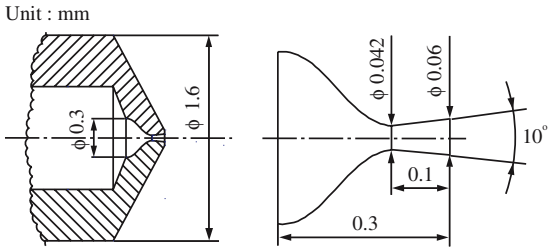

Figure 8. Schematic of the micro nozzle.

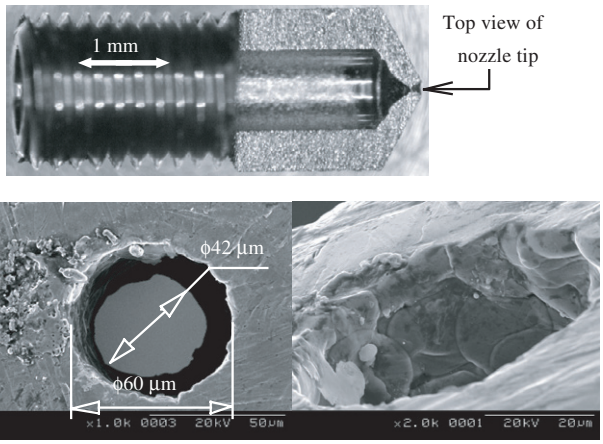

Figure 9. Microscopic image of micro nozzle (top), and SEM images of the nozzle tip; a top view (left) and a magnified view (right).

radial direction, when the total pressure is 0.1 MPa. Thus, the fuel and air will be well mixed in a relatively short distance. It is noted that larger tube length is required for complete mixing with increasing gauge total pressure corresponding to larger primary mass flow rate.

3. Fabrication

Figures 8 and 9 show the schematic, microscopic and SEM images of the present micro nozzle for the primary flow. The tip of the nozzle is designed to have a curved convergent–divergent contour, and is fabricated by high-precision electro-discharge machining (EDM) of stainless steel. Although EDM

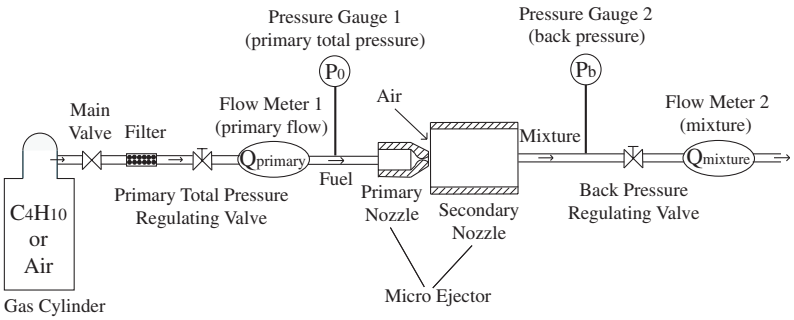

Figure 10. Experimental setup for the micro ejector.

is a well-known technique in making small-scale structurs out of metal material, fabrication of complex 3D features down to several tens of microns still remains a challenge.

If compared with MEMS ejectors having a flat chamber [10, 11], the ejector with the present nozzle has a truly 3D shape, which can be made without a complicated fabrication process. In addition, by utilizing an axisymmetric structure, the present design minimizes the viscous loss at the wall of the secondary nozzle. However, the wall surface of the present prototype nozzle is somewhat rough, and the cross-sectional shape is not a perfect circle. This is partially because electro-discharge machining from both the inlet and outlet sides is needed. Tiny particles being removed from the nozzle attach to the finished part during machining.

4. Experiment and discussion

The experimental setup for the present ejector is shown in figure 10. Butane or air stored in a gas cylinder is used for the primary flow source. Ambient air is sucked in from the inlet of the secondary nozzle. The primary total pressure and back pressure are measured by two pressure gauges (AP-13S, KEYENCE, accuracy $= \pm 1$ kPa; ISP-6-200D, SIBATA, accuracy $= \pm 1$ Pa). The primary flow rate and the flow rate of air–butane mixture are respectively measured by a thermal mass flowmeter (F-101S-A-11-N, MASFLO-OVAL, accuracy $= \pm 0.3$ sccm) and a soap film flowmeter having a low pressure drop (SF-2U, HORIBA STEC, accuracy $= \pm 5$ sccm in the measurement range of 20–200 sccm, and ± 10 sccm in the measurement range of 200–1000 sccm). The primary total pressure and back pressure are regulated by two valves.

Figures 11 and 12 respectively show the experimental results of the primary volume flow rate versus gauge total pressure for butane and air as the primary flow source. It is shown in a quasi-1D analysis that the primary flow can reach a supersonic state when the total pressure is larger than 0.071 MPa for butane, and 0.090 MPa for air. At low total pressure, the experimental data are somewhat lower than the results of the quasi-1D calculation probably due to the viscous effect. The experimental data are slightly larger than the computational results when the throat diameter is assumed to be the same as the designed value of 42 μm. However, both experimental data asymptotically approach the calculation results, when the effective throat diameter is estimated to be 43.15 μm. The results with the standard k–ε model by assuming a throat diameter of 42 μm are slightly smaller

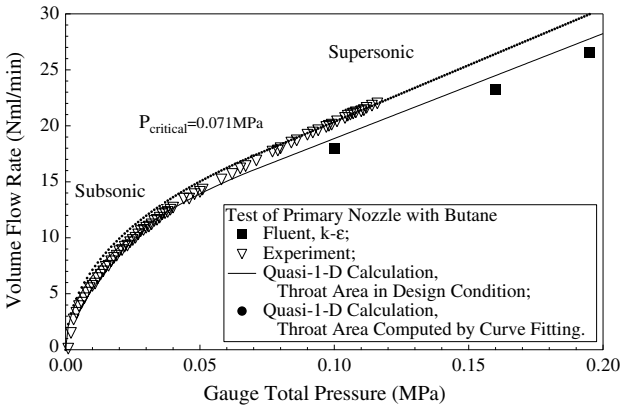

Figure 11. Effect of total pressure on the butane flow rate produced by the micro nozzle. Primary flow is butane.

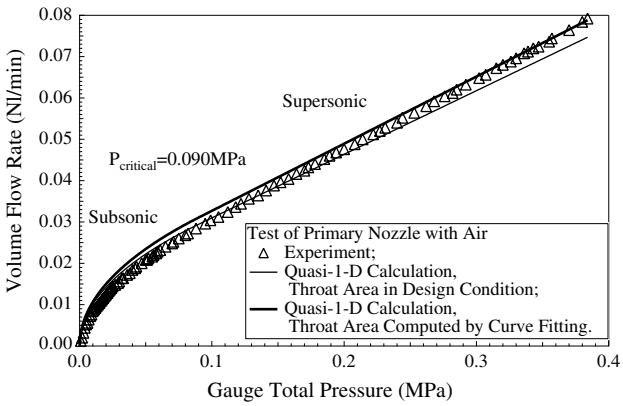

Figure 12. Effect of total pressure on the air flow rate produced by the micro nozzle. Primary flow is air.

than the results with the quasi-1D model due to the viscous effect, and the resulting displacement thickness at the throat is estimated to be around 1 μm.

As mentioned above, the area ratio is defined as the ratio of the cross-sectional area of the secondary nozzle to the exit area of the primary nozzle, and is changed by using straight circular tubes with different inner diameters (table 1). The diameter is measured by a digital vernier caliper, of which the accuracy is ± 0.02 mm.

Figure 13 shows the effect of back pressure on the volume–flow-rate ratio, which is defined as the ratio of the secondary flow rate to the primary flow rate. The flow-rate

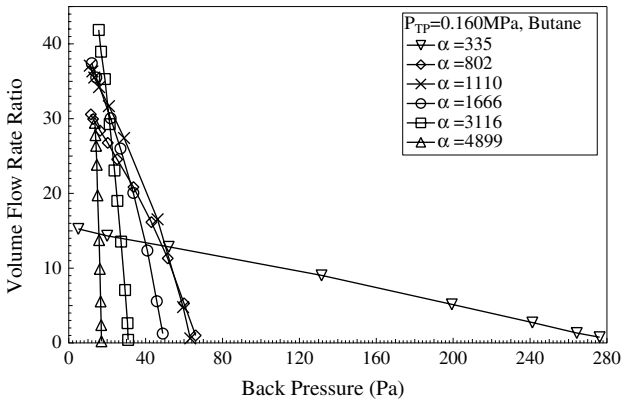

Figure 13. Volume–flow-rate ratio versus back pressure for various area ratios. Primary flow is butane.

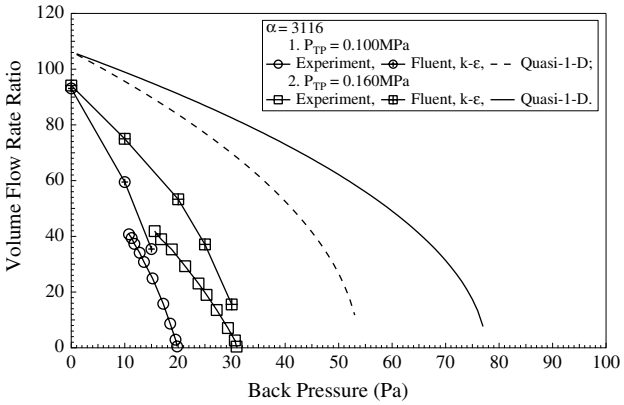

Figure 14. Comparison of volume–flow-rate ratio between computational results and the experimental data. Primary flow is butane.

Table 1. Area ratio of micro ejectors.

Exit diameter of primary nozzle	0.060						
Inner diameter of secondary nozzle	1.00	1.10	1.70	2.00	2.45	3.18	4.20
Area ratio	277	335	802	1110	1666	3116	4899

ratio reaches a maximum of 43 at a back pressure of 11.6 Pa for the ejector having an area ratio of 3116, but it rapidly decreases with increasing back pressure. Ejectors with smaller area ratios produce higher volume–flow-rate ratios for larger back pressure, but they produce lower volume–flow-rate ratios for small back pressure. In contrast, the ejector with a large area ratio produces a higher volume–flow-rate ratio for smaller back pressure, and vice versa. The present data are qualitatively in accordance with the previous data in a MEMS ejector [10, 11].

Figure 14 shows the comparison of volume–flow-rate ratios between the computational results and the experimental data. CFD results give much smaller volume–flow-rate ratios than quasi-1D computation due to viscous loss, and imperfect mixing in the ejector. Although the trends of the CFD results and the experimental data are qualitatively similar, the present experimental data for two different primary total pressures are much smaller than the CFD results. It is conjectured that this

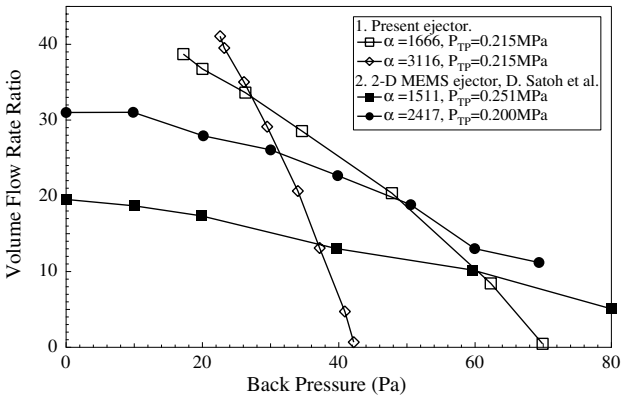

Figure 15. Comparison between present ejector and a 2D MEMS ejector [10]. Primary flow is butane.

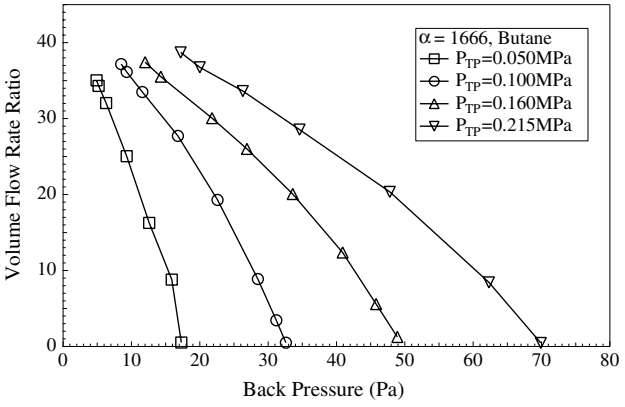

Figure 16. Volume–flow-rate ratio versus back pressure for various total pressures. Primary flow is butane.

is partially due to the rough inner surface of the present micro nozzle as shown in figure 9. In addition, the overestimation of mixing by the standard k–ε turbulence model, as mentioned above, should also account for this noncoincidence to an extent.

If compared with the 2D MEMS ejector [10] having area ratios of 1511 and 2417, the present ejector produces higher volume–flow-rate ratio for small back pressure as shown in figure 15, although the ratio is more rapidly decreased with increasing back pressure. It is conjectured that larger volume–flow-rate ratio for higher back pressure can be obtained if the secondary nozzle of the present ejector has a diffuser for pressure recovery.

It is shown in figure 16 that the increase in primary total pressure leads to larger volume–flow-rate ratio even for large back pressure. However, the maximum total pressure for n-butane is about 0.24 MPa when the gas temperature is 300 K, and the corresponding maximum back pressure where the volume–flow-rate ratio keeps above the target value of 31 is only about 30 Pa. This indicates that using fuels that can provide larger primary total pressure than butane, for example iso-butane and propane, may yield a large volume–flow-rate ratio at large back pressure [11]. The maximum total pressure for propane is about 1.2 MPa at 300 K, and the required air-to-propane ratio for stoichiometric combustion is 25, which is somewhat lower than that of butane. Because it is found

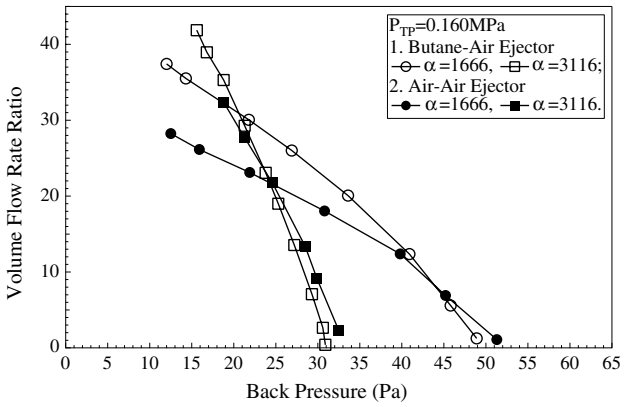

Figure 17. Comparison of air–air ejector and butane–air ejector at the same primary total pressure.

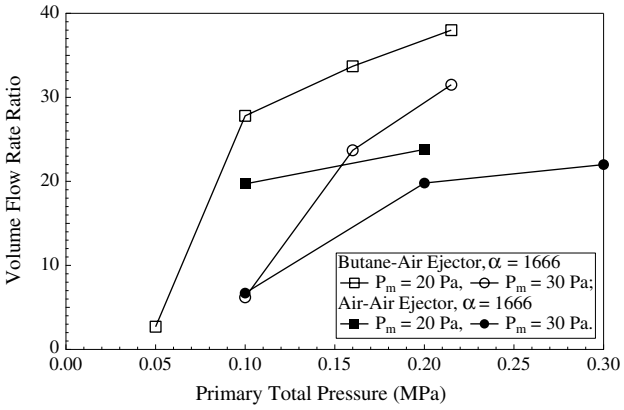

Figure 18. Comparison of air–air ejector and butane–air ejector at the same area ratio.

in the present quasi-1D computation that the mass–flow-rate ratio is insensitive to the variation of gas species, the maximum volume–flow-rate ratio for propane at the same primary static pressure should be about 76% of that of butane due to its smaller molecular weight.

To examine the effect of the molecular weight of the primary flow source on the volume–flow-rate ratio, additional experiments with air have been conducted. Figure 17 shows the effect of area ratio and back pressure for air–air and butane–air ejectors at the same primary total pressure. It is shown that for small back pressure, the volume–flow-rate ratio of the air–air ejector is much smaller, but for large back pressure, the air–air ejector produces a slightly larger volume–flow-rate ratio. For a small area ratio, the difference in the volume–flow-rate ratio between the air–air and butane–air ejectors becomes more obvious at small back pressure.

Figure 18 shows the effect of the primary total pressure on the volume–flow-rate ratio, when the area ratio is 1666. The volume–flow-rate ratio increases with increasing primary total pressure, and decreases with increasing back pressure both in the air–air and butane–air ejectors. Again, the volume–flow-rate ratio of the air–air ejector is smaller than that of the butane–air ejector due to its smaller molecular weight, which is in accordance with what can be expected from the quasi-1D calculation and also the previous data [11].

5. Conclusions

We have developed a micro ejector having an axisymmetric nozzle to supply fuel–air mixture for a micro butane combustor. High-precision electro-discharge machining is employed to fabricate a convergent–divergent supersonic nozzle, of which the throat diameter is 42 μm. The maximum volume–flow-rate ratio of 43 has been achieved for a back pressure of 11.6 Pa, which is sufficient for the stoichiometric condition, but rapidly decreases with increasing back pressure. A series of numerical simulations of the flow inside ejectors has been made with a standard k–ε turbulence model. The CFD results are in accordance with the present experimental data, but the volume–flow-rate ratio is overestimated significantly. This is partially due to the roughness of the nozzle wall surface. It is also found that the present ejector can produce a larger volume–flow-rate ratio than the previous 2D MEMS ejector at small back pressure.

Acknowledgment

This work was supported by the New Energy and Industrial Technology Development Organization (NEDO) of Japan.

References

[1] Epstein A H *et al* 1997 Micro-heat engines, gas turbines, and rocket engines—the MIT microengine project *AIAA Paper* 97-1773

[2] Fernandez-Pello A C, Fu K, Knobloch A J, Martinez F C, Walther D C, Pisano A P, Liepmann D, Maruta K and Miyasaka K 2001 Design and experimental results of small-scale rotary engine *Proc. 2001 Int. Mechanical Engineering Congr. and Expo. (IMECE), ASME publication IMECE/MEMS-23924*

[3] Palo D R, Holladay J D, Rozmiarek R T, Guzman-Leong C E, Wang Y, Hu J, Chin Y-H, Dagle A and Baker E G 2002 Development of a soldier-portable fuel cell power system: Part I. A bread-board methanol fuel processor *J. Power Sources* **108** 28–34

[4] Lu G Q and Wang C T 2005 Development of micro direct methanol fuel cells for high power applications *J. Power Sources* **144** 141–5

[5] Schaevitz S, Franz A J, Jensen K F and Schmidt M A 2001 A combustion-based MEMS thermoelectric power generator *Proc. 11th Int. Conf. on Solid-State Sensors and Actuators (Munich)* pp 30–3

[6] Suzuki Y, Horii Y, Kasagi N and Matsuda S 2004 Micro catalytic combustor with tailored porous alumina *Proc. 17th IEEE Int. Conf. MEMS2004 (Maastricht)* pp 312–5

[7] Okamasa T, Lee G G, Suzuki Y and Kasagi N 2005 Development of micro catalytic combustor using ceramic tape casting *Proc. 5th Int. Workshop on Micro and Nanotechnology for Power Generation and Energy Conversion Applications (Power MEMS 2005, Tokyo)* pp 206–9

[8] Presz W Jr, Reynolds G and Hunter C 2002 Thrust augmentation with mixer/ejector systems *AIAA Paper* 2002-0230

[9] Harrell G and Kornhauser A 1995 Performance tests of a two-phase ejector *IECEC* Paper Number 95-69

[10] Satoh D, Tanaka S, Yoshida K and Esashi M 2005 Micro-ejcector to supply fuel–air mixture to a micro-combustor *Sensors Actuators* A **119** 528–36

[11] Tanaka S, Chang K S, Min K B, Satoh D, Yoshida K and Esashi M 2004 MEMS-based components of a miniature fuel cell/fuel reformer system *Chem. Eng. J.* **101** 143–9

[12] Dutton J C and Carroll B F 1986 Optimal supersonic ejector designs *Trans. ASME, J. Fluids Eng.* **108** 414–20
[13] Lewis D H, Janson S W Jr, Cohen R B and Antonsson E K 2000 Digital micropropulsion *Sensors Actuators* A **80** 143–54
[14] Kohler J, Bejhed J, Kratz H, Bruhn F, Lindberg U, Hjort K and Stenmark L 2002 A hybrid cold gas microthruster system for spacecraft *Sensors Actuators* A **97–98** 587–98
[15] Bayt R L and Breuer K S 2000 Fabrication and testing of micron-sized cold-gas thrusters *Micropropulsion for Small Spacecraft, Progress in Aeronautics and Astronautics* vol 187 ed M Micci and A Ketsdever (Washington, DC: AIAA Press) pp 381–97
[16] Lempert W R, Boehm M, Jiang N, Gimelshen S and Levin D 2003 Comparison of molecular tagging velocimetry data and direct simulation Monte Carlo simulations in supersonic micro jet flows *Exp. Fluids* **34** 403–11
[17] Wang M and Li Z 2004 Performance predictions of MEMS-based nozzles at moderate or low temperatures *Proc. 2nd Int. Conf. Microchannels and Minichannels (ICMM2004)* pp 731–8
[18] Hao P, Ding Y, Yao Z, He F and Zhu K 2005 Size effect on gas flow in micro nozzles *J. Micromech. Microeng.* **15** 2069–73
[19] Launder B E and Spalding D B 1972 *Lectures in Mathematical Models of Turbulence* (London: Academic)
[20] Myong H K and Kasagi N 1990 A new approach to the improvement of k–ε turbulence model for wall-bounded shear flows *JSME Int. J.* II **33** 63–72
[21] Tennekes H and Lumley J L 1972 *A First Course in Turbulence* (Cambridge, MA: MIT Press)